ELSEVIER

Constraints on the post ~25-ka slip rate of the Yammoûneh fault (Lebanon) using in situ cosmogenic ^{36}Cl dating of offset limestone-clast fans

Mathieu Daëron[a,*], Lucilla Benedetti[b], Paul Tapponnier[a], Alexandre Sursock[c], Robert C. Finkel[d]

[a]Laboratoire de Tectonique, Institut de Physique du Globe de Paris, 4 place Jussieu, 75252 Paris Cedex 05, France
[b]UMR 6635, Centre Européen de Recherche et d'Enseignement des Géosciences de l'Environnement, BP 80,
Europôle Méditerranéen de l'Arbois, 13545 Aix-en-Provence Cedex 4, France
[c]Centre National de Géophysique, Conseil National de la Recherche Scientifique, P.O. Box 165432, Ashrafieh, 1100-2040, Beirut, Lebanon
[d]Center for Accelerator Mass Spectrometry, Lawrence Livermore National Laboratory, L-206, 7000 East Ave, Livermore, CA 94550, USA

Abstract

The most active seismogenic structure along the eastern shore of the Mediterranean is the N–S-trending left-lateral Levant Fault System (LFS), the plate boundary between Arabia and Africa. In Lebanon, it forms a 160-km-long restraining bend responsible for the uplift of Mount Lebanon. The resulting transpression is partitioned between the offshore Tripoli–Roûm thrust and the Yammoûneh strike–slip fault. There are few quantitative constraints on the Quaternary slip rate along the LFS. Here we present a direct estimate of the ~25-ka mean slip rate on the Yammoûneh fault. Mapped offsets of alluvial fans at two sites ~50 km apart on the eastern flank of Mount Lebanon range between 24 ± 2 and 80 ± 8 m. About 30 limestone cobbles sampled on these fans yield in situ cosmogenic ^{36}Cl exposure ages mostly between 6 and 27 ka. A statistical assessment of offsets versus ages provides bounds on the Late Pleistocene–Holocene slip rate on the fault: 3.8–6.4 mm/yr. These results are consistent with long-term geological inferences, confirming that the Yammoûneh fault is the main strike–slip branch of the LFS in Lebanon. They illustrate both the potential and the difficulties of using in situ cosmogenic ^{36}Cl dating of limestone-clast fan deposits for deciphering tectonic and geomorphic processes in the Mediterranean.
© 2004 Published by Elsevier B.V.

Keywords: Levant fault; active faulting; cosmogenic nuclides; Cl-36

---

1. Introduction

Stretching from the Gulf of Aqaba to the Eastern Anatolian Fault System, the Levant Fault System (LFS) connects the Red Sea spreading center to the collisional belt of southeastern Turkey (Fig. 1A). This ~1000-km-long left-lateral transform fault accommodates the relative motion between the Arabian and Nubian plates [1–3]. That simple picture is complicated by the presence of the Sinai microplate [4–7], comprising the Sinai peninsula and the Levantine margin, and by internal deformation of the Arabian plate, most notably within the Palmyrides fold belt.

Direct knowledge of the slip rate along the LFS is thus essential to a quantitative understanding of the plate kinematics of Arabia, Nubia and the Sinai block.

This slip rate is currently uncertain by more than a factor of 2 over time periods from 18 Myr to 10 yr (Table 1). In addition, the geometry and kinematics of the LFS are better understood south of Lake Tiberias (Gulf of Aqaba and Dead Sea fault) than to the north.

Plate motion reconstructions for Arabia and Nubia based on the analysis of seafloor spreading recorded by magnetic anomalies in the Red Sea [8] predict 5.6–11 mm/yr of left-lateral motion in the 4°E direction in Lebanon, but also about 2.4–3.7 mm/year of E–W shortening (Table 1). GPS measurements over the past 10 years are compatible with these results in terms of Euler poles and rotation rates [7]: the GPS-predicted N–S strike–slip rate in Lebanon is ~4.0–8.1 mm/yr, with ~2.8–3.7 mm/yr of strike-perpendicular (E–W) shortening (Table 1). Rates calculated from both the
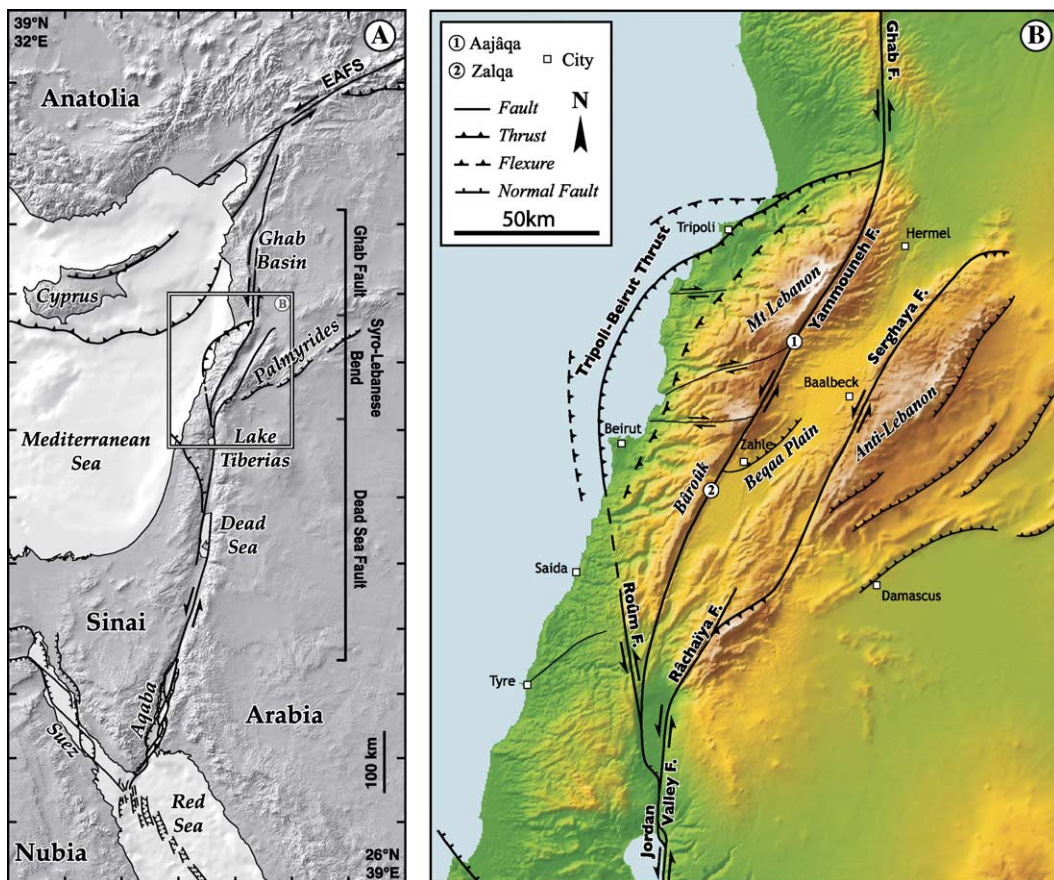

Fig. 1. (A) Map of Levant fault system. Box shows limits of panel B. Faulting in Red Sea (including gulfs of Aqaba and Suez) is from Courtillot et al. [4]; "EAFS"="East Anatolian Fault System." (B) Active faults of Lebanese re-straining bend. Circled numbers mark locations of studied sites: Aajâqa (1) and Zalqa (2).

Table 1
Various estimations of slip rate along the LFS

Slip rate (along-strike, mm/yr)	Time span	Method	References
>5.8	<18 Myr	Geological offsets	Freund et al. [2], Garfunkel [3]
8.5±0.5	~5 Myr	Geological offsets	Freund et al. [2], Garfunkel [3]
8.4±2.8	3.2 Myr	Red Sea seafloor spreading	Chu and Gordon [8]
4.0±2.0	>25 kyr	Geomorphology (Araba valley)	Klinger et al. [10]
6.9±0.1	~2 kyr	Paleoseismology (Missyaf, Syria)	Meghraoui et al. [12]
6.0±2.0	10 yr	GPS	McClusky et al. [7]

Only strike–slip component predicted in Lebanon (34°N, 36°E) on LFS is shown. Both seafloor spreading and GPS models assume no significant motion between Sinai and Nubia and predict transpressive slip north of Lake Tiberias, all the way to triple junction with EAFS.

seafloor spreading and GPS models assume no significant movement between Nubia and the Sinai block. It is generally acknowledged, however, that such motion does exist [4,7,8], although it remains poorly constrained. Reliable estimates of the slip rate along the LFS therefore require geological and geomorphic field studies or local GPS profiles. It has long been recognized that the total left-lateral slip on the southern LFS is ~105 km and postdates 18 Ma [2–4,9], which yields a minimum long-term slip rate of ~5.8 mm/yr (Table 1). Cumulative slip over the last 5 Myr, as recorded by offset Late Miocene to Early Pliocene geological markers between Zahle and the Dead Sea [2,3], is about 40–45 km, which implies a faster slip rate of 8–9 mm/yr over this period (Table 1).

Over a shorter time span, cumulative offsets of U/Th, [10]Be and ^{14}C-dated Mid-Pleistocene to Holocene alluvial surfaces and fans in the Araba valley, between Aqaba and the Dead Sea, record an average slip rate of 2–6 mm/yr over the past 140±31 ka along the main branch of the Dead Sea fault [10], similar to that previously inferred by Ginat et al. [11] (3–7.5 mm/yr). In Syria, Meghraoui et al. [12] used paleoseismologic and archeologic evidence to propose an average slip rate of 6.9±0.1 mm/yr along the Missyaf segment of the Ghab fault over the past ~2000 years. This result is, however, based on cumulative slip due to only three earthquakes. Using

such a small number of seismic cycles to extrapolate to geological time scales may give rates that differ significantly from the actual mean Holocene or Pleistocene slip rate.

The aim of this study is to provide more quantitative constraints for Late Pleistocene–Holocene slip rates. We targeted the Yammoûneh fault, the main strike–slip branch of the LFS in the Lebanese restraining bend. Based on cosmogenic [36]Cl surface exposure dating of limestones cobbles in young alluvial fans, we have determined the age of cumulative offsets at two sites along the fault about 50 km apart (Fig. 1B). The morphology of each area was accurately mapped by combining field observations with evidence from stereoscopic air photographs, topographic maps and satellite imagery in order to measure horizontal offsets. We describe below the sampling strategy and the method for exposure age calculation, and how we derive a mean slip rate on the fault over ~25 ka.

2. Geomorphic offsets along the Yammoûneh fault

2.1. Active faulting in the Lebanese restraining bend

Along most of its length, the LFS is transtensional, with large-scale pull-apart structures such as the Gulf of Aqaba, Dead Sea, Lake Tiberias and Ghab basins (Fig. 1A). By contrast, between 33°N and 34.5°N, about halfway along its length, the Levant fault's trace veers by ~25° along a 160-km-long right-stepping restraining bend, long held responsible for crustal shortening and mountain building in Lebanon. In this region (Fig. 1B), the Levant fault splits into three branches, with clear evidence for slip partitioning: the two easternmost strands (Yammoûneh and Râchaïya–Serghaya) are left-lateral strike–slip faults, while the WNW–ESE shortening associated with the restraining bend is taken up on a previously unrecognized offshore fault, the Tripoli–Roûm Thrust, which dips ESE under Mount Lebanon [13].

Geologically and geomorphically, the Yammoûneh fault appears to be the main on-land branch of the LFS. It marks the boundary between Mount Lebanon, 3090 m a.s.l., and the Beqaa plain, 1000 m a.s.l. (Fig. 1B). Its 160-km-long surface trace is sharp and clear in the topography. We mapped it in the field, using aerial and satellite imagery. North of Zahle, it cuts

across Cretaceous limestones, whereas to the south, it marks the contact between Jurassic limestones (the Bâroûk ridge) to the west and younger Cretaceous, Tertiary or Quaternary rocks. The ~30°E fault strike does not vary much, except in the vicinity of small (≤6 km long) basins or ridges, which form small-scale pull-aparts or pushups. Though the fault's seismogenic potential is still a matter of debate, it lies fully within the isoseismals of the *M*>7 earthquake of 1202 AD [14,15].

All along its trace, the fault commonly offsets Quaternary landforms such as river channels, small gullies and fans. We describe below the morphology and Quaternary geology of two such sites, 50 km apart (Fig. 1B), where offset alluvial fans offer clear evidence of cumulative slip.

2.2. Site 1: offset fans in the Yammoûneh Basin

The Yammoûneh basin lies 1400 m a.s.l., on the eastern flank of Mount Lebanon, between thick subtabular sequences of karstified Cenomanian limestone. This 6-km-long, 2-km-wide depression is the largest pull-apart basin along the fault, to which it gives its name. The modern, active surface trace of the fault cuts across the basin. At the north end of the pull-apart, as it veers away from the basin's western rim, the active fault cuts and offsets two alluvial fans built by short, steep catchments that erode the limestone range front (Fig. 2).

Fig. 3 shows our map of the fans' surface geology and morphology, and of the trace of the fault, based on field observations, stereoscopic air photographs at a scale of 1/25,000, topographic maps (1/20 000) and QuickBird satellite images (60-cm resolution). In each fan, several distinctive surfaces stand out. Although it is clear that, overall, the fans are offset left-laterally by the fault, the original topography, particularly of the lowest, most gently sloping parts of each fan, has been modified by agricultural terracing. The resulting blur of most limits precludes measuring cumulative offsets, except for the northern fan (Aajâqa fan), whose NE edge is well-defined, providing a piercing line.

To assess the cumulative offsets and corresponding uncertainties, both the geomorphic map of Fig. 3 and the satellite image were retro-fitted (Fig. 4). Back-slipping along the fault restores the continuity and linearity of different types of geomorphic markers at
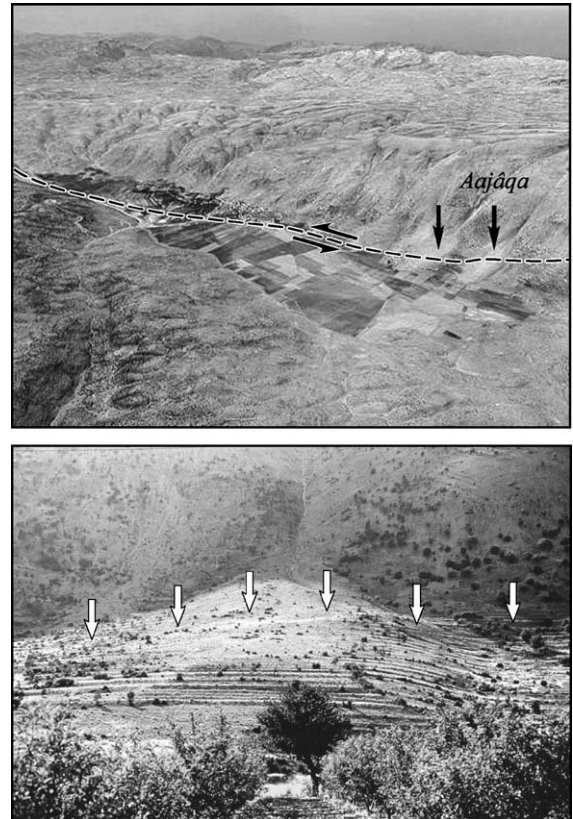

Fig. 2. Aerial view of Yammoûneh basin (upper panel). Basin originally formed as active pull-apart, but there is no visible strike–slip faulting on either side. Instead, as inferred from resistivity measurements [35] and confirmed by recent paleoseismologic studies [36], active fault now shortcuts pull-apart. We studied offsets of two fans (black arrows) in northernmost part of basin. Field view of Aajâqa fan in Yammoûneh basin (lower panel). Distal (sunlit) part of fan is offset left-laterally by Yammoûneh fault (white vertical arrows) with respect to fan apex.

this site, providing different values of cumulative offset. A back-slip of 24±2 m is necessary to restore a shallow gully incised into the surface of the Aajâqa fan. Pairing this offset with the age of the incised surface would only yield a strict lower bound on the slip rate. With ~35 m of back-slip, the alignment between the fan's feeder channel west of the fault and the NW–SE-trending fan axis (*A*) is restored. Because of high-energy deposition at the base of a steep, 45° slope, this axis is uniquely defined as the only rectilinear streamline of the topographic gradient; as expected, it strikes parallel (134°E) to the fan's feeder channel, all the way down to the basin floor. Finally,
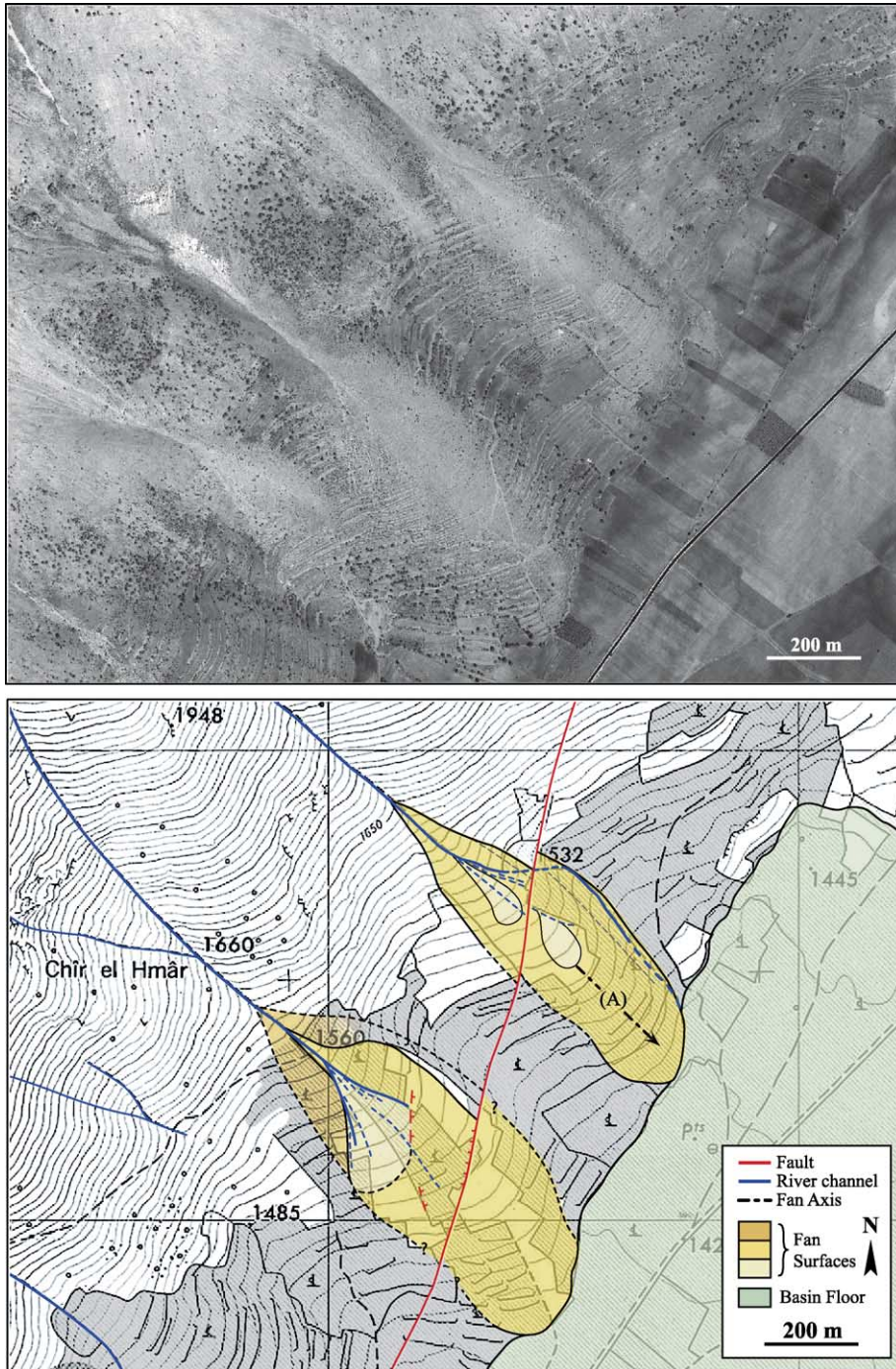
Fig. 3. (Top) QuickBird satellite image of two northern fans in Yammoûneh basin. (Bottom) Corresponding map. Distinct surfaces of different ages are shown within each fan. Full lines limit extent of fan deposits, while dashed lines mark inflexion of topography where range-front slope meets curved fan surface. Cumulative offsets are similar for both fans, although only northernmost one (Aajâqa fan) shows piercing line offsets clear enough to yield quantitative results. A is Aajâqa fan's topographic axis (see text).
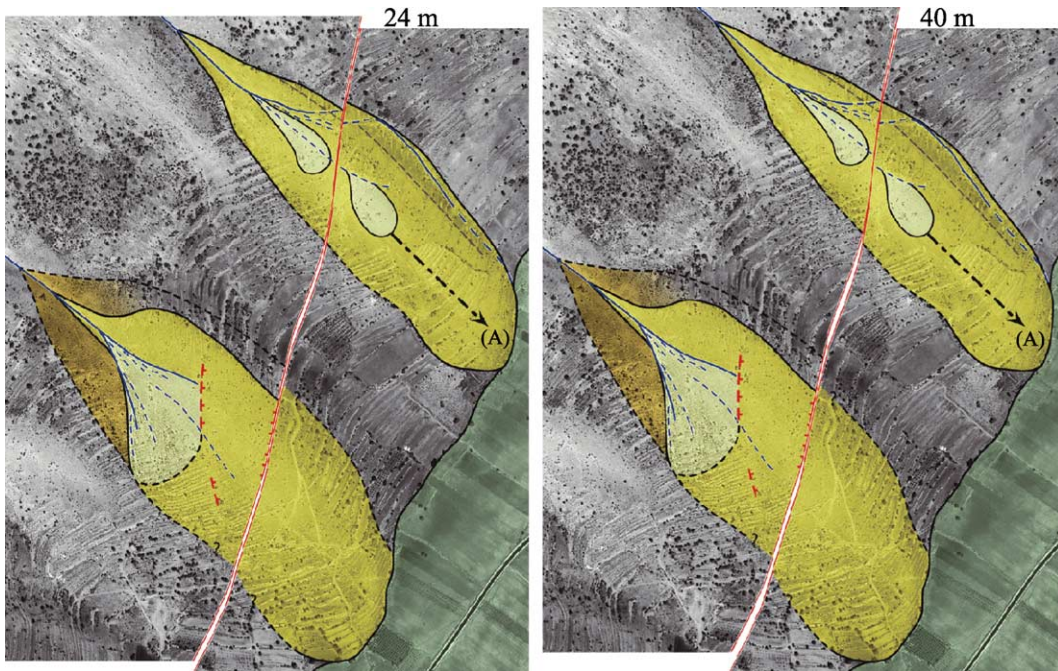
Fig. 4. Retro-fit of Yammoûneh fans. (Left) 24±2 m of backward slip restores median incision on surface of Aajâqa fan. (Right) 40±5 m of backward slip restores NE edge of Aajâqa fan. Slightly smaller amount of back-slip (~35 m) restores alignment of Aajâqa fan's feeder channel and fan's axis.

40±5 m of back-slip is needed to restore the NE edge of the fan, which is unquestionably the best defined of the three offset markers. We conclude that the cumulative offset of the fan surface is most likely between 35 and 45 m. Although all the deposits on that surface may not have been emplaced at the same time, dating the main episode(s) of aggradation should yield bounds on the slip rate.

2.3. Site 2: offset of the Zalqa fan

Fig. 5 shows a west-looking view of the Zalqa fan, 50 km south of the Yammoûneh basin. It lies ~900 m a.s.l. on the west side of the Beqaa plain (cf. Fig. 1B) at the base of the steep east-facing flank of the southern tip of Mount Lebanon (Bâroûk anticline). It is a well-developed, 1-km-wide alluvial fan composed of limestone pebbles, cobbles and boulders. The fan's conic envelope is truncated near its apex and offset left-laterally with respect to its feeder channel. The main difference between this site and the Yammoûneh site is that here, the fault cuts mostly across the limestone bedrock at the fan apex rather than across the fan.

Fig. 6 shows our map of the Zalqa site. Upstream from the fault, three channels (C1, C2 and C3) have fed the fan. C1 and C2 merge near the top of the fan apex. C1 (Ouâdi Zalqa) has the broadest catchment and has incised deepest. Its channel is filled with weakly weathered limestone debris, distinctive on the air
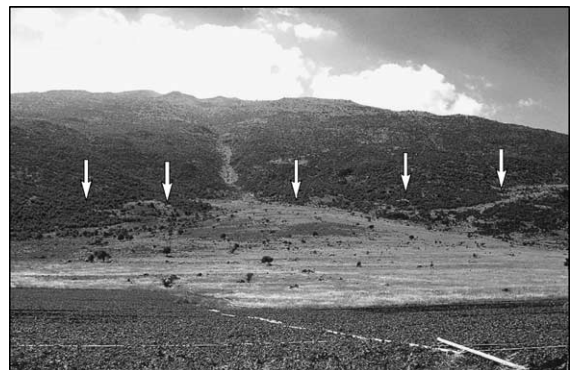

Fig. 5. Field view of the Zalqa fan. Bulk of fan deposit is not aligned with main feeder channel due to cumulative left-lateral slip on Yammoûneh Fault (white vertical arrows), which cuts fan just below its apex (cf. Fig. 6).
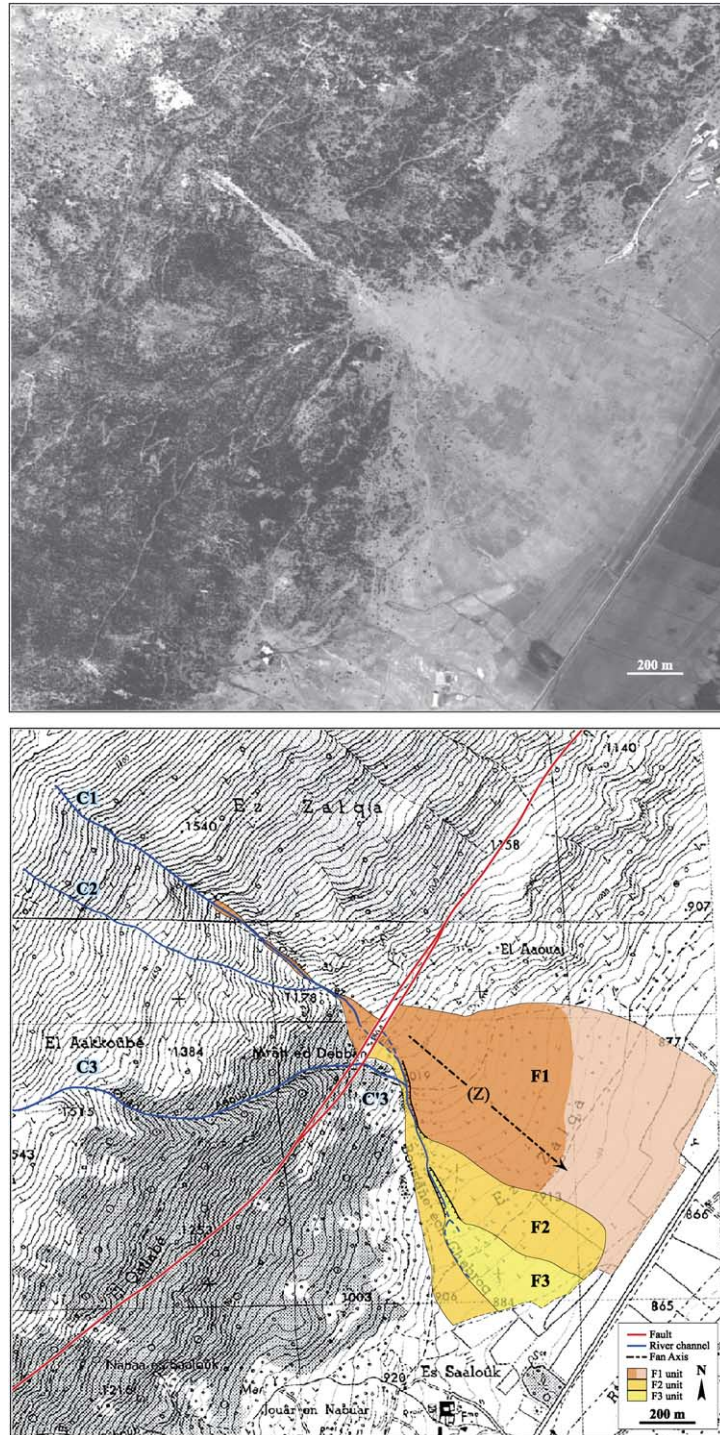
Fig. 6. (Top) Spot-5 satellite image of Zalqa fan. (Bottom) Corresponding map. Three fan generations with different surfaces and ages (F1, F2 and F3) are mapped. Oldest F1 surface is clearly offset by Yammoûneh fault. Note recent capture of channel C3. Z is topographic axis of F1 (see text).

photos and Spot 5 image from their light color. These observations strongly suggest that C1 is the main feeder channel of the Zalqa fan. The third channel C3 (Ouâdi Aaouaj), is located south of the two others and presently crosses the fault with no visible offset. We interpret this to indicate that it was recently captured by the small C′ 3 stream west of the fan. This inference is supported by the deepening of incision in the C3–C′ 3 channel downstream from the fault zone.

The Zalqa fan is composed of three subunits (F1, F2 and F3). F1 is the largest and oldest. It extends from the fan apex tip to the cultivated flats in the Beqaa. Its upper half is steeper and more cone-shaped than its distal part. A younger unit F2, inset at a lower level, was later emplaced along the SW side of F1. Later still, F2 was incised by a new channel which fed the lowest and youngest fan F3. It is unclear which feeder channel was primarily responsible for this latest aggradation event, although C3 was certainly involved.

The Yammoûneh fault's active trace cuts F1 ~100 m downslope from the fan apex tip. Cumulative displacement juxtaposed the top of F2 next to the apex of F1. Similarly, it brought F1 into contact with the Jurassic limestone bedrock of the mountain's flank. The trace of the fault splays into two parallel strands, ~20 m apart, across the fan apex. Fig. 7 shows retro-

fitted maps of the Zalqa fan. The restorations are performed using air photographs, topographic maps (1/20,000), Spot 5 (2.5-m resolution) and Ikonos (1-m resolution) images.

As at the previous site, two different values of cumulative offset are recorded. Back-slip of 40 ± 2 m is required to realign a small but well-defined channel incision on the surface of F1. Again, however, there is no reliable way to date the incision itself, except that it must postdate the emplacement of F1. Back-slip of 80 ± 8 m restores the geometry of the apex of F1, as well as the alignment between C1 and the topographic axis (Z) of F1's upper conic surface (defined as at Aajâqa). The consistency between these two fits strongly suggests that ~80 m is the cumulative offset since the aggradation of F1.

3. Cosmogenic dating of offset alluvial fans

3.1. Chlorine-36 surface exposure dating of limestone cobbles

Cosmogenic exposure dating of alluvial fans has so far mostly been applied to surfaces bearing silicate-rich rocks (e.g. [16–18]). In Lebanon, as in much of

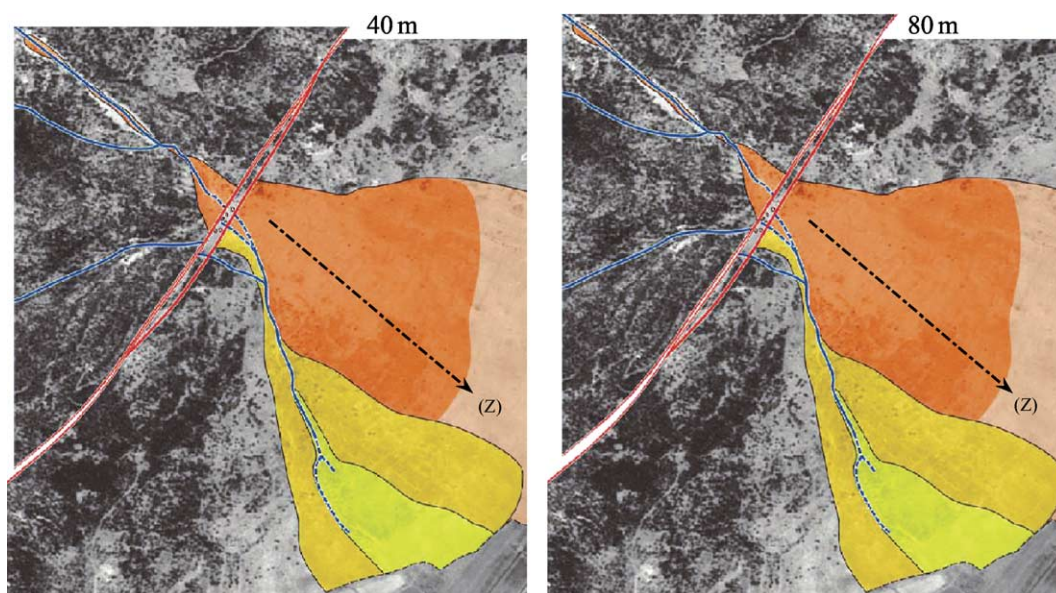

Fig. 7. Retro-fit of Zalqa site. (Left) 40 ± 2 m of backward slip restores narrow channel incised in F1. (Right) 80 ± 8 m of backward slip restores outer edges of F1 and alignment between upstream feeder channel and topographic axis Z.

the Mediterranean, however, limestone rocks are ubiquitous. Here we used [36]Cl to determine the surface exposure age of the limestone cobbles that pave the surface of the two alluvial fans described above. In limestone, [36]Cl is produced primarily through interactions of cosmic ray secondary neutrons and muons with Ca in calcite ($CaCO_3$) (e.g. [19,20]). The production rate decreases exponentially with depth and [36]Cl is thus mostly accumulated near the surface [21]. In general, the accumulation of cosmogenic nuclides in a rock exposed at the earth surface may be described by [22]:

$$N(t) = N(0)e^{-\lambda t} + \frac{P}{\lambda + \varepsilon\mu}\left(1 - e^{-(\lambda+\varepsilon\mu)t}\right)$$

where $N(t)$ is the concentration at time t (year), P is the surface production rate (atom/g/yr), λ is the decay constant of the radioactive nuclide (2.303×10^{-6} yr^{-1} for [36]Cl), is the erosion rate (cm/yr) and μ is the absorption coefficient (cm^{-1}), equal to ρ/L, where ρ is the density of the sampled rock (here 2.7 g/cm^3 since our samples are nearly pure calcite according to [Ca] measurements) and L is the absorption mean free path for interacting cosmic secondary particles in the rock (160 g/cm^2). $N(0)$ is the inheritance component.

Our goal is to date geomorphic features that have been passively preserved during displacement along the fault. The geomorphic freshness of the Aajâqa and Zalqa alluvial fans suggests that they are young enough that the effects of erosion at the surface might be expected to be small. Recent studies in the Mediterranean show that hanging bedrock carbonate

surfaces can be lowered by dissolution at rates of between 8 [23] and 29 μm/yr [20]. How these estimates can be extrapolated to gently sloping alluvial surfaces, however, remains unclear. Karstic dissolution typically increases surface relief on horizontal scales of up to several meters and leads to consolidation by calcite cementation of the clasts. Neither of the fan surfaces we sampled shows significant relief at such scales, and the angular limestone clasts and cobbles are loose, with interstitial clay only, down to depths of at least 2 m (Aajâqa) and 70 cm (Zalqa). Moreover, on both surfaces, cobbles show little evidence of dissolution, such as microkarst, pits, etc. (Fig. 8). Finally, there is no evidence that the cobbles now at the surface might have been buried tens of centimeters deep under shallower cobbles now removed by dissolution. For instance, none of the cobbles show remnant clay-rich concretion patches typical of long underground burial. Hence, although we cannot completely rule out that some dissolution affected the surface of the fans, we find it likely that the amount has been too small to have a significant effect.

The rather short and steep catchments of both Ouâdi Zalqa and Ouâdi Aajâqa imply short transport times and little along-stream storage. Systematic observations in similar catchments elsewhere have shown that this configuration usually yields sample populations that, despite variable inheritance, are often characterized by sample ages that show a cluster at the youngest end of the age distribution. This young cluster typically has the same age as that, independently determined by radiocarbon dating, for the

Fig. 8. (A) Typical cobble sampled on Zalqa fan; (B) surface and depth profile on Aajâqa fan (see text).

abandonment of the alluvial surface (e.g. [16,17,24]). In other words, most samples show negligible systematic inheritance, but a few, which have had more complex transport histories, show much older ages and can be regarded as outliers. In view of the rather steep slopes of the fans (~8–10°), however, superficial rearrangement of the cobbles after initial emplacement cannot be ruled out. Also, we cannot rule out that parts of the fan surfaces have a composite nature, resulting from somewhat diachronous periods of deposition.

Fourteen limestone cobbles were collected and dated on each fan. The altitudes and locations of the samples were measured with a handheld GPS. We therefore estimate the uncertainty on horizontal and vertical positions to be ~15 m and at least 20 m, respectively. We selected cobbles of about the same size (20–30 cm diameter), well embedded in the ground (i.e. protruding a few centimeters above the surface, cf. Fig. 8), to minimize the possibility of post-emplacement disturbances.

After grinding, leaching and chemical extraction of chlorine by precipitation of silver chloride, the ^{36}Cl and chloride concentration in the carbonate was determined for all samples by isotope dilution accelerator mass spectrometry at the Lawrence Livermore National Laboratory CAMS facility. Blanks were 2 orders of magnitude lower than the samples and replicates agreed to better than 5%.

3.2. Results

Surface exposure ages were calculated using the ^{36}Cl production rates from calcium of Stone et al. [25] for all relevant pathways. Other published production rates—e.g. Swanson and Caffee [26] and other references therein—are greater than Stone et al.'s value, which would lead to ages younger by about 20%. The production rates were calculated at our site latitude and altitude using Lal [22] coefficients. The exposure ages presented in Table 2 include analysis and processing errors, as well as the error on Stone et al.'s production rate. Shielding by the surrounding topography was measured in the field and found to be negligible.

At both sites, there seems to be little systematic relationship between ^{36}Cl concentration and sample position, although at Aajâqa, three of the oldest samples are located in the distal part of the fan. A 2-m-deep depth profile (Fig. 8) dug in the central part of the Aajâqa fan, east of the fault, yielded ^{36}Cl concentrations that did not show the expected decrease as a function of depth consistent with single-stage deposition of a homogeneous population of cobbles.

The surface ages ranges between 4.0 ± 0.3 and 27.3 ± 2.1 kyr at Aajâqa and between 7.8 ± 0.9 and 66.0 ± 6.9 kyr at Zalqa (Table 2 and Figs. 9 and 10). Even though the data show a fair amount of scatter at both sites, groups of ages can be discerned, with clusters of young ages. At Aajâqa, 7 samples out of 14 are between 5.7 and 9.6 ka, and 5 are between 13 and 22 ka. Two samples do not belong to these two groups: Y18 (3.9 ka) and Y3 (27 ka). At Zalqa, sample ages are generally older, with 4 out of 14 between 12 and 15 ka, and 6 between 19 and 27 kyr. ZLQ-W4 (7.8 ka) is younger by 4 kyr than the youngest sample of the first group. By comparison with other terraces and fans dated with cosmogenic isotopes elsewhere (e.g. [17,24]), we interpret ZLQ-E8 (35 ka), E1 (45 ka) and E9 (66 ka), which are much older than the oldest sample of the second group, to have experienced exposure before deposition (inheritance) and therefore consider them to be outliers.

In order to discuss these data further, we plotted in Fig. 10 the sum at each site of the Gaussian age probability distributions (P_{sum}) for all dated samples [27], expressed as [28]:

$$P_{\text{sum}}(t) = \sum_i \mathrm{e}^{-(t-a_i)^2/2\sigma_i^2}/\sigma_i\sqrt{2\pi}$$

where t is time, a_i is the exposure age of sample i and ($2\sigma_i$) is the reported error. The two curves show distinct peaks that quantify the grouping of samples by age inferred from simple inspection of the data and support our elimination of the three oldest Zalqa samples as outliers. Fig. 10 demonstrates the temporal coincidence of the three main distribution peaks (~20, ~14 and ~8 ka) at both sites. Such correspondence, in regions ~50 km apart, argues for successive emplacement episodes of distinct cobble populations. Hence, although we cannot rule out the possibility of scatter or bias due to loss of chlorine by alteration or erosion of cobbles, or by postdepositional burial or exhumation, our results are in favor of fan aggradation controlled by regional climate, leading to successive

Table 2
Sample characteristics and exposure ages

Sample	Altitude (m)	Latitude (°N)	Ca dissolved (g)	Chlorine (ppm)	^{36}Cl [atoms (g rock)$^{-1}$]	^{36}Cl production rate [atoms (g rock)$^{-1}$ yr^{-1}]	Age (yr)
Y18	1541	34.15	4.82	10.2	187 065 ± 10 046	46.9	3990 ± 327
Y19	1544	34.15	9.32	38.6	264 822 ± 10 246	46.2	5730 ± 419
Y1	1442	34.15	9.50	7.5	261 183 ± 9938	43.2	6040 ± 464
Y5	1489	34.15	12.17	28.5	332 484 ± 10 756	48.2	6903 ± 498
Y17	1539	34.15	6.89	7.3	371 688 ± 15 029	47.1	7894 ± 586
Y8	1494	34.15	6.23	22.3	378 593 ± 16 710	45.0	8409 ± 657
Y11	1513	34.15	8.06	10.1	428 412 ± 15 962	47.5	9026 ± 663
Y6	1491	34.15	10.89	23.4	438 796 ± 11 568	45.4	9655 ± 672
Y14	1539	34.15	11.12	23.0	674 586 ± 17 797	50.2	13 432 ± 909
Y4	1445	34.15	11.00	29.9	686 618 ± 18 370	44.5	15 442 ± 1106
Y2	1442	34.15	9.82	20.1	844 814 ± 22 629	44.1	19 148 ± 1376
Y9	1503	34.15	7.70	25.5	997 896 ± 29 756	48.0	20 783 ± 1467
Y16	1536	34.15	9.45	45.0	1 095 443 ± 28 919	50.1	21 883 ± 1484
Y3	1442	34.15	4.58	19.2	1 201 051 ± 41 877	44.0	27 323 ± 2057
ZLQ-W4	1091	33.2	14.06	28.2	319 323 ± 28 375	41.0	7782 ± 921
ZLQ-E12	1049	33.2	15.41	14.3	455 219 ± 39 863	38.6	11 794 ± 1405
ZLQ-W1	1067	33.2	15.75	20.0	494 880 ± 43 486	39.4	12 569 ± 1490
ZLQ-E7	973	33.2	15.73	14.7	469 079 ± 39 237	36.7	12 786 ± 1527
ZLQ-E3	947	33.2	15.81	22.3	535 036 ± 36 105	36.0	14 874 ± 1638
ZLQ-W3	1083	33.2	15.17	36.1	734 847 ± 39 617	39.2	18 761 ± 1792
ZLQ-E11	1056	33.2	13.65	22.2	722 007 ± 48 401	37.9	19 050 ± 1994
ZLQ-E5	961	33.2	15.27	33.0	765 504 ± 48 884	37.4	20 491 ± 2198
ZLQ-E10	1055	33.2	16.19	17.4	843 703 ± 70 037	39.1	21 572 ± 2493
ZLQ-E6	969	33.2	15.38	29.0	871 437 ± 78 153	36.4	23 911 ± 2966
ZLQ-E2	941	33.2	15.71	20.8	963 681 ± 66 638	35.8	26 914 ± 3002
ZLQ-E8	972	33.2	15.73	19.4	1 309 400 ± 80 555	37.3	35 117 ± 3705
ZLQ-E1	943	33.2	13.12	16.9	1 593 818 ± 119 858	35.6	45 192 ± 5244
ZLQ-E9	967	33.2	16.89	12.8	2 376 936 ± 144 957	36.0	66 049 ± 6947

Scaling factors for ^{36}Cl production by neutrons and muons were calculated at each site (see [21,25] and references therein). Calcium content in each sample was measured by ICP at CEREGE, with respective average Ca/(g rock) contents of 37 ± 1% at Zalqa and 35 ± 1% at Aajâqa. ^{36}Cl measurements were standardized relative to a NIST ^{36}Cl standard.

emplacement episodes of distinct cobble populations, as documented elsewhere (e.g. [17,23]). This fan emplacement scenario is in agreement with the conclusion of Klinger et al. [29], who relate main aggradation periods in the Dead Sea area, ~350 km to the south, to warm and wet pluvials before the Younger Dryas, between 15 and 13 ka (cf. 15–12 ka peak at Zalqa in Fig. 10) and around 7 ka (cf. youngest peak at Aajâqa in Fig. 10).

The observed offsets cannot predate the onset of aggradation. Alternatively, one could argue that the entire offset accrued since aggradation stopped and the fan became passive. To estimate the slip rate on the Yammoûneh fault, we choose to use these guidelines to set conservative bounds and take the recorded age of the offsets to be within the bounds of the latest

major aggradation episodes, as reflected by the relative weight of age clusters on each fan (Fig. 10): at Aajâqa, half of the sample ages cluster within 6–10 kyr, while at Zalqa, most were emplaced between 27 and 12 ka.

3.3. Slip rate

At Aajâqa, 40 ± 5 m of slip would thus have been recorded since at most ~10 ka and at least ~6 ka, while at Zalqa, 80 ± 8 m of slip would have accrued since at most ~27 ka and at least ~12 ka (Fig. 11). The rates obtained are 3.5–7.5 mm/yr at Aajâqa and 2.7–7.3 mm/yr at Zalqa.

These ranges of values are fully consistent, as they should be, given the similar orientation of the fault at
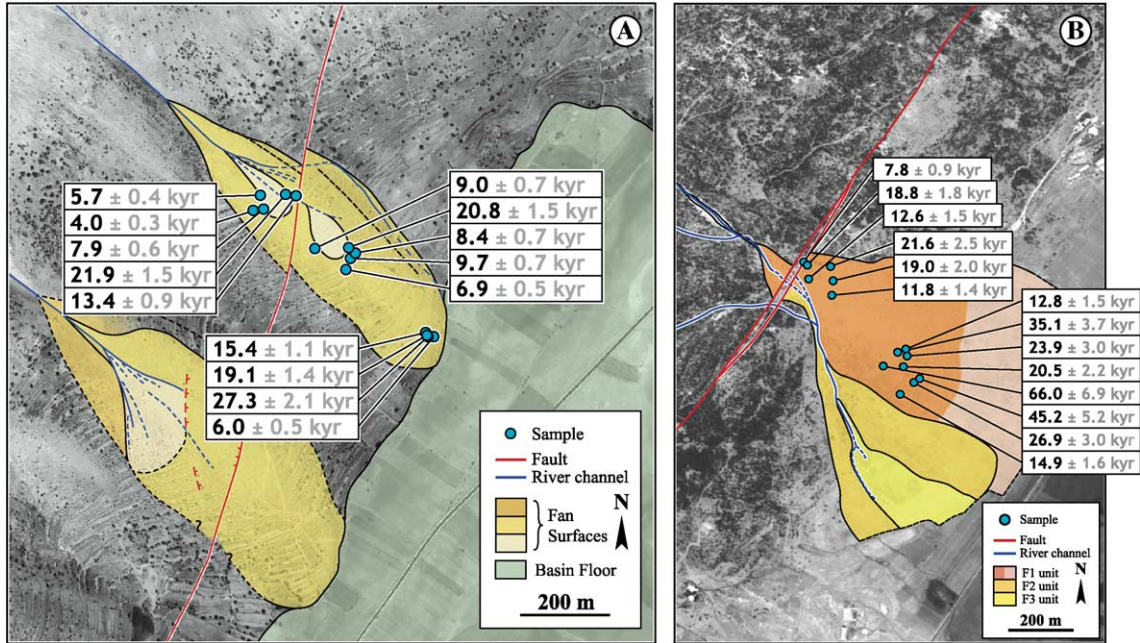
Fig. 9. Position and exposure ages of dated limestone cobbles on offset Aajâqa (A) and Zalqa (B) fans. Little relationship is visible between sample position and exposure age, although old samples tend to be in distal parts of fans.
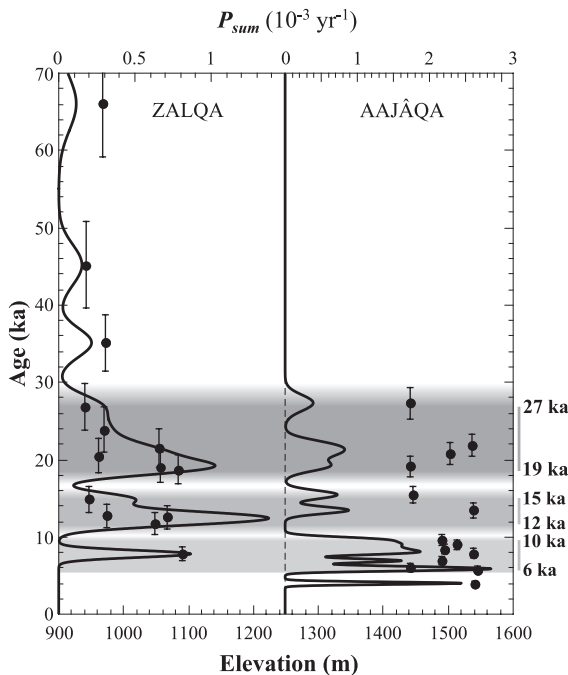

Fig. 10. Exposure ages of samples, with corresponding error bars, plotted versus sample elevation (cf. Table 2). Curves are age probability sums (see text).

both sites and its simple geometry in between. It is therefore legitimate to combine both data sets to further constrain the bounds on the slip rate by multiplying the two rate probability distributions. At each site, we take the age (a) of the offset to have a uniform probability distribution between its lower and upper bounds a_{min} and a_{max} (5.73–9.65 ka at Aajâqa and 11.8–26.9 ka at Zalqa). The value (d) of the offset has a Gaussian probability distribution whose center (d_o) and σ-value (σ_d) are such that the 95% confidence intervals are, respectively, 35–45 m (Aajâqa) and 72–88 m (Zalqa).

The probabilities for d and a being independent, the rate ($v=d/a$) probability distribution at each site can be written as:

$$P_v(v) = \frac{1}{\sigma_d \sqrt{2\pi}(a_{max} - a_{min})} \times \int_{a_{min}}^{a_{max}} \exp\left(-\frac{(vt - d_o)^2}{2\sigma_d^2}\right) t\,dt$$

and the combined probability distribution for v is the normalized product of the two distributions (Fig. 11).
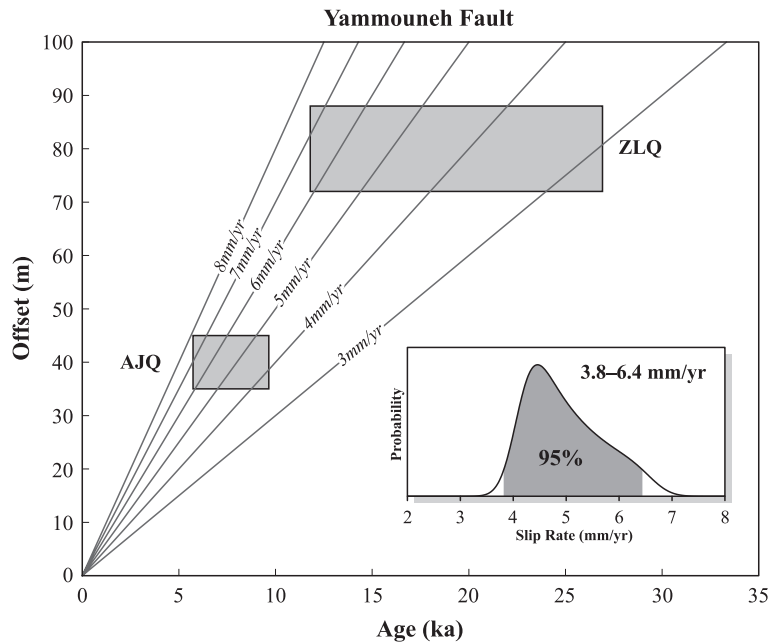
Fig. 11. Constraints on slip rate of Yammoûneh Fault. Plot of offsets versus ages shows consistency of results at Aajâqa (AJQ) and Zalqa (ZLQ). Inset shows corresponding probability distribution of slip rate on Yammoûneh fault (see discussion in text).

The 95% confidence interval for this combined distribution argues for a slip rate within 3.8–6.4 mm/yr. In conclusion, in the Late Pleistocene–Holocene, the slip rate along the Yammoûneh fault appears to be 5.1±1.3 mm/yr.

4. Summary and discussion

Quantitative geomorphic evidence at two distinct sites yields the first direct geological estimate of the Late Pleistocene–Holocene slip rate on the Yammoûneh fault, 5.1±1.3 mm/yr. This estimate is derived from ^{36}Cl surface exposure ages of offset alluvial fans, assuming zero erosion of the fan surfaces, as supported by field evidence, and zero systematic inheritance, as documented in several other cosmogenic studies of similar sites (e.g. [16,17,23,30]). Clearly, stronger erosion would imply older exposure ages, hence slower slip rates, while unaccounted inheritance would have the opposite effect.

Our result is consistent with Mio-Pliocene constraints. Additionally, in contrast with the claims of other authors [31–33], it confirms that the Yammoûneh fault is the main strike–slip branch of the

Levant Fault System in the Syro-Lebanese restraining bend.

Since the Yammoûneh fault is only one of three subparallel strands of the LFS in Lebanon, however, it is less straightforward to compare our recent slip rate with those proposed by previous authors to the north and south. The difference between the rate of 5.1±1.3 mm/yr that we find and the rate of 6.9±0.1 mm/yr inferred along the Missyaf segment of the northern LFS in Syria by Meghraoui et al. [12] may be explained in two ways. First, the time span of our study is ~25 kyr, as opposed to ~2 kyr at Missyaf. Second, the two study areas are separated by a triple junction at the northern tip of Mount Lebanon (Fig. 1), where the NE termination of the Tripoli–Roûm thrust connects back with the Yammoûneh fault. Kinematically, the slip rate on the LFS should increase north of that junction.

Comparison with the results of Klinger et al. [10] in southern Jordan is even more delicate. Although the slip rate (4±2 mm/yr) they obtain along the Araba segment of the southern LFS is, within errors, consistent with ours, at least three first-order fault junctions (with the Roûm, Râchaïya and Carmel faults) separate Mount Lebanon from the Araba

valley, ~400 km to the south. Slip on any of these active faults should significantly change the rate on the LFS. Both the Roûm and Râchaïya faults are left-lateral, so that the slip rate south of Lake Tiberias is expected to be faster than along the Yammoûneh fault. Gomez et al. [34], for instance, estimated a slip rate of 1.4 ± 0.2 mm/yr along the Serghaya fault, northern continuation of the Râchaïya fault. A similar kinematic effect should occur with the Carmel fault, a NW-striking normal fault. In keeping with Klinger et al.'s value, a southward-decreasing slip rate on the LFS might result from counterclockwise rotation of the Sinai–Levant micro-plate, with a Euler pole relative to Arabia somewhere in northern Egypt or in the southern Levantine basin. This would diminish the left-slip component along the LFS in the south and move the northern Levantine basin (west of Lebanon and SE of Cyprus) away from Arabia, consistent with the direction of subduction SE of Cyprus. Besides, this might explain why the northern LFS shows no sign of strike-perpendicular compression north of Mount Lebanon, contrary to the predictions of most Nubia–Arabia motion models [7,8].

Comparison of our results with the post-Miocene mean slip rate on the southern LFS (8–9 mm/yr), provided that it is representative of the Late Pleisto-cene–Holocene period, suggests that the Yammoûneh fault accounts for over one-half of the north–south motion along the Levant fault in Lebanon. Clearly, better constraints on the longer-term (Pleistocene) slip rate along the Yammoûneh fault are required. Similarly, more work needs to be done on the other Lebanese faults to determine their Late Pleistocene–Holocene rates and to better understand the slip partitioning and crustal deformation processes at work within the restraining bend.

References

[1] R. Freund, A model of the structural development of Israel and adjacent areas since Upper Cretaceous times, Geological Magazine 102 (1965) 189–205.
[2] R. Freund, I. Zak, Z. Garfunkel, Age and rate of the sinistral movement along the Dead Sea rift, Nature 220 (1968) 253–255.
[3] Z. Garfunkel, Internal structure of the Dead Sea leaky transform (rift) in relation to plate kinematics, Tectonophysics 80 (1981) 81–108.
[4] V. Courtillot, R. Armijo, P. Tapponnier, The Sinai triple junction revisited, Tectonophysics 141 (1987) 181–190.
[5] A. Salamon, A. Hofstetter, Z. Garfunkel, H. Ron, Seismicity of the eastern Mediterranean region: perspective from the Sinai subplate, Tectonophysics 263 (1996) 293–305.
[6] J. Mascle, J. Benkhelil, G. Bellaiche, T. Zitter, J. Woodside, L. Loncke, Marine geologic evidence for a Levantine–Sinai plate, a new piece of the Mediterranean puzzle, Geology 28 (2000) 779–782.
[7] S. McClusky, R. Reilinger, S. Mahmoud, D. Ben Sari, A. Tealeb, Gps constraints on Africa (Nubia) and Arabia plate motions, Geophysical Journal International 155 (2003) 126–138.
[8] D. Chu, R.G. Gordon, Current plate motions across the Red Sea, Geophysical Journal International 135 (1998) 313–328.
[9] A.M. Quennell, Tectonics of the dead sea rift, Proceedings of the 20th International Geological Congress, Mexico, 1959, pp. 385–403.
[10] Y. Klinger, J.-P. Avouac, N. Abou Karaki, L. Dorbath, D. Bourles, J.-L. Reyss, Slip rate on the Dead Sea transform fault in northern Araba valley Jordan, Geophysical Journal International 142 (2000) 755–768.
[11] H. Ginat, Y. Enzerl, Y. Avni, Translocated Plio-Pleistocene drainage systems along the Arava fault of the Dead Sea transform, Tectonophysics 284 (1998) 151–160.
[12] M. Meghraoui, F. Gomez, R. Sbeinati, J. Van der Woerd, M. Mouty, A.N. Darkal, Y. Radwan, I. Layyous, H. Al Najjar, R. Darawcheh, F. Hijazi, R. Al-Ghazzi, M. Barazangi, Evidence for 830 years of seismic quiescence from palaeoseismology, archaeology and historical seismicity along the Dead Sea fault in Syria, Earth and Planetary Science Letters 210 (2003) 35–52.
[13] P. Tapponnier, M. Daëron, G. King, E. Jacques, A. Sursock, A. Elias, Active faulting and seismic hazard in Lebanon, Journal of Conference Abstracts 6 (2001)1988 (EUG XI abstracts).

[14] N.N. Ambraseys, C.P. Melville, An analysis of the eastern Mediterranean earthquake of 20 May 1202, in: W.K.H. Lee, H. Meyers, K. Shimazaki (Eds.), History of Seismography and Earthquakes of the World, Academic Press, San Diego, CA, 1988, pp. 181–200.

[15] R. Ellenblum, S. Marco, A. Agnon, T. Rockwell, A. Boas, Crusader castle torn apart by earthquake at dawn, 20 May 1202, Geology 26 (1998) 303–306.

[16] J. Van der Woerd, F.J. Ryerson, P. Tapponnier, Y. Gaudemer, R. Finkel, M. Caffee, Zhao Guoguang, He Qunlu, Holocene left slip-rate determined by cosmogenic surface dating on the Xidatan segment of the Kunlun Fault (Qinghai, China), Geology 26 (1998) 695–698.

[17] J. Van der Woerd, P. Tapponnier, F.J. Ryerson, A.-S. Mériaux, B. Meyer, Y. Gaudemer, R.C. Finkel, M.W. Caffee, Zhao Guoguang, Xu Zhiqin, Uniform postglacial slip-rate along the central 600 km of the Kunlun Fault (Tibet), from ^{26}Al, ^{10}Be, and ^{14}C dating of riser offsets, and climatic origin of the regional morphology, Geophysical Journal International 148 (2002) 356–388.

[18] J.F. Ritz, D. Bourlès, E.T. Brown, S. Carretier, J. Chery, B. Enhtuvshin, P. Galsan, R.C. Finkel, T.C. Hanks, K.J. Kendrick, H. Philip, G. Raisbeck, A. Schlupp, D.P. Schwarz, F. Yiou, Late Pleistocene to Holocene slip rates for the Gurvan Bulag thrust fault (Gobi-Altay, Mongolia) estimated with ^{10}Be dates, Journal of Geophysical Research 108 (B3) (2003).

[19] L. Benedetti, R. Finkel, D. Papanastassiou, G. King, R. Armijo, F. Ryerson, D. Farber, F. Flérit, Post-glacial slip history of the Sparta fault (Greece) determined by ^{36}Cl cosmogenic dating: evidence for non-periodic earthquakes, Geophysical Research Letters 29 (8) (2002) 1246.

[20] S.G. Mitchell, A. Matmon, P.R. Bierman, Y. Enzel, M. Cafee, D. Rizzo, Displacement history of a limestone normal fault scarp, northern Israel, from cosmogenic ^{36}Cl, Journal of Geophysical Research 106 (B3) (2001) 4247–4264.

[21] J.O.H. Stone, G.L. Allan, L.K. Fifield, R.G. Cresswell, Cosmogenic chlorine-36 from calcium spallation, Geochimica et Cosmochimica Acta 60 (4) (1996) 679–692.

[22] D. Lal, Cosmic ray labelling of erosion surfaces: in situ nuclide production 13 rates and erosion models, Earth and Planetary Science Letters 104 (1991) 424–439.

[23] L. Benedetti, R. Finkel, G. King, R. Armijo, D. Papanastassiou, F.J. Ryerson, F. Flérit, D. Farber, G. Stavrakakis, Motion on the Kaparelli fault (Greece) prior to the 1981 earthquake sequence determined from ^{36}Cl cosmogenic dating, Terra Nova 15 (2003) 118–124.

[24] A.-S. Mériaux, F.J. Ryerson, P. Tapponnier, J. Van der Woerd, R.C. Finkel, X. Xu, Z. Xu, M.W. Caffee, Rapid slip along the central Altyn Tagh fault: morphochronologic evidence from Cherchen He and Sulamu Tagh, Journal of Geophysical Research 109 (B6) (2004).

[25] J.O.H. Stone, J.M. Evans, L.K. Fifield, G.L. Allan, R.G. Cresswell, Cosmogenic chlorine-36 production in calcite by muons, Geochimica et Cosmochimica Acta 63 (3) (1998) 433–454.

[26] T.W. Swanson, M.L. Caffee, Determination of ^{36}Cl production rates derived from the well-dated deglaciation surfaces of Whidbey and Fidalgo Islands, Washington, Quaternary Research 56 (2001) 366–382.

[27] T.V. Lowell, The application of radiocarbon age estimates to the dating of glacial sequences: an example from the Miami sublobe, Ohio, USA, Quaternary Science Reviews 14 (1995) 85–99.

[28] J.R. Taylor, An Introduction to Error Analysis, The Study of Uncertainties in Physical Measurements, second edition, University Science Books, Sausalito, CA, 1997.

[29] Y. Klinger, J.-P. Avouac, D. Bourles, N. Tisnerat, Alluvial deposition and lake-level fluctuations forced by Quaternary climate change: the Dead Sea case example, Sedimentary Geology 162 (2003) 119–139.

[30] A.-S. Mériaux, Détermination par datation cosmogénique des variations de la vitesse de glissement sur la faille de l'Atlyn Tagh depuis 100 ka. PhD thesis, Univ. Paris VII, 2002.

[31] R.W.H. Butler, S. Spencer, H.M. Griffiths, Transcurrent fault activity on the Dead Sea Transform in Lebanon and its implications for plate tectonics and seismic hazard, Journal of the Geological Society (London) 154 (1997) 757–760.

[32] R.W.H. Butler, S. Spencer, Landscape evolution and the preservation of tectonic landforms along the northern Yammoûneh Fault, Lebanon, in: B.J. Smith, W.B. Whalley, P.A. Warke (Eds.), Uplift, Erosion and Stability: Geological and Geomorphological Perspectives on Landscape Evolution, Spec. Publ. Geol. Soc. London 162 (1999) 143–156.

[33] K. Khair, Geomorphology and seismicity of the Roum fault as one of the active branches of the dead sea fault system in Lebanon, Journal of Geophysical Research 106 (B3) (2001) 4233–4246.

[34] F. Gomez, M. Merghraoui, A.N. Darkal, F. Hijazi, M. Mouty, Y. Souleiman, R. Sbeinati, R. Darawcheh, R. Al-Ghazzi, M. Barazangi, Holocene faulting and earthquake recurrence along the Serghaya branch of the Dead Sea fault system in Syria and Lebanon, Geophysical Journal International 153 (2003) 658–674.

[35] J. Besançon, Le poljé de Yammoûné, Hannon 3 (1968) 3–62.

[36] M. Daëron, P. Tapponnier, E. Jacques, A. Elias, G. King, A. Sursock, R. Gèze, A. Charbel, Evidence for Holocene slip and large earthquakes on the Yammoûneh fault (Lebanon). In EOS, Transactions, AGU, 82 (47), 2001. Fall Meet. Suppl., Abstract S52D-0666.